Journal of Volcanology and Geothermal Research 424 (2022) 107504

Contents lists available at ScienceDirect

Journal of Volcanology and Geothermal Research

journal homepage: www.journals.elsevier.com/journal-of-volcanology-and-geothermal-research

Petrology of Koko Rift basalts: Hawai'i's most recent and atypical rejuvenation stage eruptive sequence

Michael O. Garcia [a,*], Kierstin Swanson [a], Charline Lormand [a,b], Marc D. Norman [c]

[a] Department of Earth Sciences, University of Hawai'i, 96822 Honolulu, HI, USA
[b] Department of Earth Sciences, Durham University, United Kingdom
[c] Research School of Earth Sciences, Australian National University, Canberra, Australia

ARTICLE INFO

Keywords:
Hawaii
Rejuvenated volcanism
Koko Rift
Geochemistry
Magma mixing

ABSTRACT

Rejuvenated volcanism is a worldwide phenomena occurring on many volcanic oceanic islands in all of the major ocean basins (e.g., Samoa, Madeira, Mauritius). This plume-related volcanism follows the main edifice-building stage after a hiatus of variable duration (e.g., 0.6–2 Myrs in Hawai'i). Hawaiian rejuvenated basalts typically have high MgO contents (>10 wt%) and carry upper mantle xenoliths. Thus, these magmas are assumed to have ascended rapidly through the crust. The basalts erupted along the Koko Rift in Honolulu, Hawai'i are unusual in their large range in MgO (5.4–11.4 wt%), absence of mantle xenoliths and history of magma mixing. The Koko Rift is the youngest area of rejuvenated volcanism in Hawai'i (67 ± 2 ka) and its best developed rejuvenation-stage rift system (15-km long rift with 12 major and several minor subaerial and submarine eruptive centers). Here we report on the first systematic petrologic investigation of the Koko Rift basalts to better understand this most recent example of Hawaiian rejuvenated volcanism. New textural and mineral chemical evidence indicates magma was stored along the rift and later mixed to produce the subaerial lavas with 10–11 wt% MgO. The lower MgO (5–6 wt%) subaerial lavas were probably byproducts of the initial hybrid magma, subsequent crystal fractionation and then a second magma mixing event. The absence of mantle xenoliths in Koko Rift lavas and the relatively moderate forsterite contents (84–85%) in the higher MgO lavas may be related to the development of a crustal magma system within the rift. The record of crustal magma storage and crystal fractionation, and two magma mixing episodes in the Koko Rift lavas is unique among Hawaiian rejuvenated volcanism.

1. Introduction

Rejuvenated volcanism is an enigmatic aspect of hotspot magmatism occurring hundreds of kilometers downstream from the ascending mantle plume stem and following a significant eruptive hiatus. Many oceanic island groups display rejuvenated volcanism including Samoa (Wright and White, 1987), Kerguelen (Weis et al., 1998), the Canary Islands (Hoernle and Schmincke, 1993), Mauritius (Paul et al., 2005) and Hawai'i (Macdonald et al., 1983). In Hawai'i, the Koko Rift is a spectacular and the most recent example of rejuvenated stage volcanism (Jicha et al., 2022). It is part of the Honolulu Volcanics, a classic example of rejuvenated volcanism (Dana, 1890). The Honolulu Volcanics formed on the ~2–3 Ma Ko'olau shield volcano after an eruptive hiatus of ~1.3 Myr (Ozawa et al., 2005). Honolulu volcanism occurred over a period of ~0.7 Myr (~0.07–0.8 Ma) and produced at least 42 monogenetic cones (e.g., Ozawa et al., 2005; Clague et al., 2016; Jicha et al., 2022).

Four parallel rifts oriented orthogonal to the propagation trend of the Hawaiian Islands were identified based on vent locations for the Honolulu Volcanics (Stearns and Vaksvik, 1935; Winchell, 1947; Jackson and Wright, 1970). The presence of orthogonal rifts played an important role in attempts to explain rejuvenated volcanism from flexural loading of the lithosphere by rapidly growing shield volcanoes (e.g., Bianco et al., 2005). However, many of the vents along these supposed Honolulu rifts are unrelated in composition and time (for compositions and ages of these eruptions, see Clague and Frey, 1982 and Ozawa et al., 2005).

The Koko Rift (Fig. 1) is a striking example of rejuvenation stage volcanism and has been referred to as the "most important group of late volcanic features on O'ahu" (Wentworth, 1926). It is a 15-km long rift with 12 major and several minor eruptive centers making it Hawai'i's best developed rejuvenation stage rift system (Fig. 2). The eruptive

* Corresponding author.
E-mail address: mogarcia@hawaii.edu (M.O. Garcia).

https://doi.org/10.1016/j.jvolgeores.2022.107504
Received 22 October 2021; Received in revised form 1 February 2022; Accepted 11 February 2022
Available online 15 February 2022

styles and deposits of the Koko Rift embody the typical characteristics of Hawaiian rejuvenated volcanism, i.e., explosive tuff cones to pillow basalts. However, the Koko Rift eruptions are atypical among Honolulu Volcanics deposits in having a wide range in MgO (5.2–12.7 wt%), weakly alkalic compositions and no mantle xenoliths (Winchell, 1947; Clague et al., 2006). Other Honolulu basalts typically have high MgO (>12 wt%), moderately to strongly alkaline compositions, and contain mantle-derived xenoliths of peridotite, dunite and/or pyroxenite (e.g., Jackson and Wright, 1970; Clague and Frey, 1982). These features led to a hypothesis that Honolulu magma rose quickly from the mantle without crustal storage (e.g., Clague, 1987). The compositional diversity of the Koko rift basalts provides an exception to this model. Here we present the first systematic petrologic investigation of Koko Rift basalts with the goal of better understanding this most recent example of Hawaiian rejuvenated volcanism.

2. Koko Rift geology

The Koko Rift formed on the southeast corner of the island of O'ahu (Fig. 1). The name Koko is Hawaiian for 'blood'. Legend reports that a man was bitten by a shark in the Koko area (Pukui et al., 1976). The Koko Rift has two segments: a 8.8 km long subaerial portion with seven major vents and numerous subsidiary vents, and a ~ 6 km long submarine ridge that extends along a trend parallel to the subaerial section but offset 0.5 km to the east (Fig. 2). The subaerial section can be subdivided into a northern section that was characterized by effusive eruptions and a southern section with predominately explosive eruptions. The submarine ridge was first recognized by Stearns and Vaksvik (1935) from a U.S. Coast and Geodetic Survey nautical chart (4110). This ridge was largely ignored until it was surveyed by Dartnell and Gardner (1999). Their map shows that the ridge consists of at least five cones (Fig. 2). The two deepest and smallest cones on the ridge were sampled via submersible by Clague et al. (2006). We sampled by dredging a larger cone just to the north of these smaller cones. Volcanism along the Koko Rift is thought to have been c*onsanguineous* (e.g., Wentworth, 1926; Winchell, 1947; Clague et al., 2006).

The northern end of the subaerial Koko Rift has three vents (Kalama, Kaupo and Kāohikaipu) that were built higher on the flanks of Ko'olau volcano (Fig. 1). These vents produced subaerial flow fields that are now partially drowned by the ocean. These drowned flows would have been subaerial when erupted (~67 ± 2 ka; Jicha et al., 2022) because global sea level was ~100 m lower at that time then it is today (e.g., Satow et al., 2021). Kalama is the largest subaerial lava flow in the Koko Rift system (Fig. 2). We estimated its volume using surface geology, U.S. Geological Survey records for 10 water wells that penetrated the flow, and lidar images and bathymetry data of the shallow ocean (<50 m) to approximate the extent of the flow offshore. These results indicate the Kalama flow is ~4 km long, 3.5 km wide and had a maximum thickness of at least 31 m (Fig. S1). A minimum volume of 0.11 km^3 (not adjusted for dry rock equivalent, DRE, given its wide variations in vesicularity; 20–45 vol%) was calculated using ArcGIS software. This is the first attempt to estimate the volume of a Honolulu Volcanics flow. The Kalama flow is comparable in volume to some of the short duration (<5 day) eruptions of Kīlauea volcano (Macdonald et al., 1983). Compared to the monogenetic Auckland volcanic field volcanoes (a better comparison for the monogenetic Honolulu volcanism), Kalama is similar in volume to some of Auckland's larger flows (e.g., Mt. Eden at 0.11 km^3; 0.084 km DRE), which were estimated to have taken several months to erupt (Kereszturi et al., 2014). The Kalama flow is much smaller than the largest Auckland flow (Rangitoto, ~0.8 km^3; Kereszturi et al., 2014).

The southern subaerial section of Koko Rift was built on the lower flanks of Ko'olau volcano. It includes the 368 m tall Koko Crater (the tallest cone among the Honolulu Volcanics), Hanauma Bay (a nested, double tuff ring complex that was subsequently breached by the ocean), Kahauloa (a tuff ring) and numerous subsidiary craters on Koko Head all formed by explosive eruptions (e.g., Nono'ula; Fig. 1). Coral reef

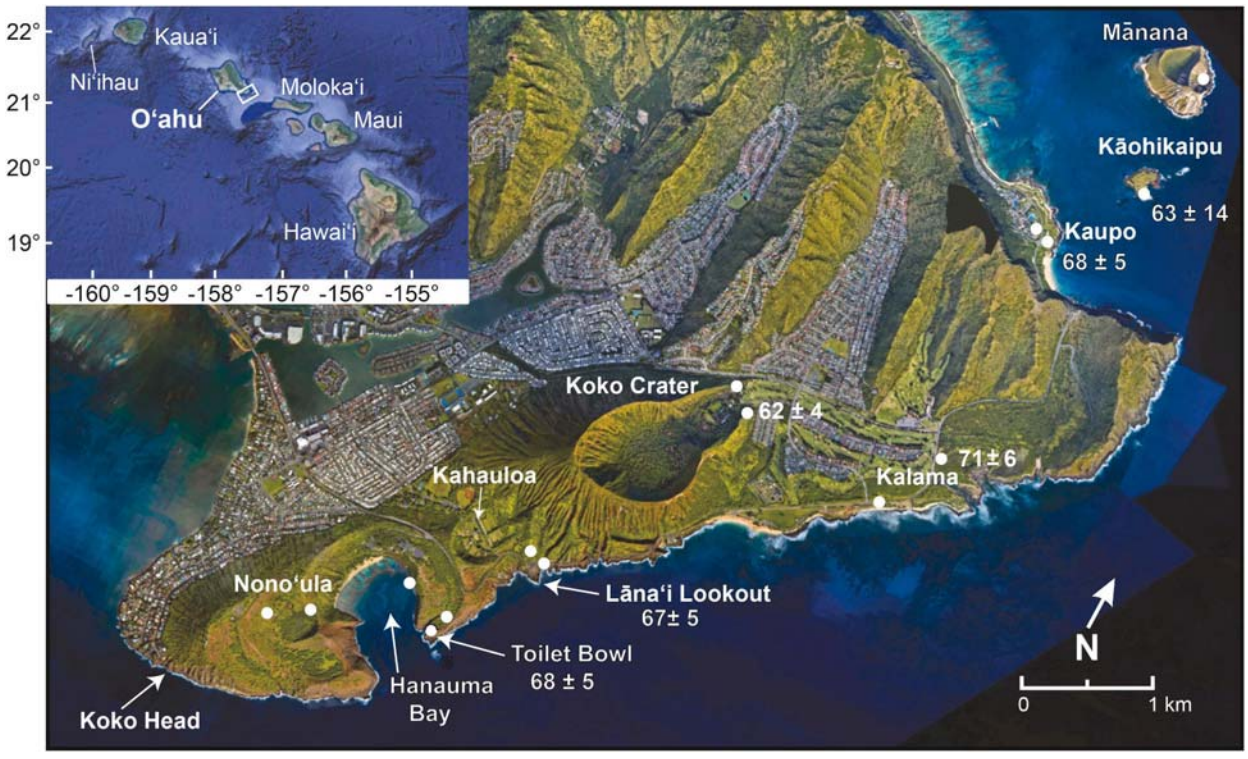

Fig. 1. Google Earth image of subaerial Koko Rift showing locations where samples were taken (white dots) and the Ar—Ar ages (ka) for dated samples (Jicha et al., 2022). A weighted mean of 14 new plateau ages from the six dated sites is 66.5 ± 2.1 ka (MSWD = 1.05). Insert map shows the Hawaiian Islands with a white rectangle indicating the Koko Rift area on the southeast corner of the island of O'ahu.

fragments are common in the tephra from these cones as are basaltic fragments from the underlying Koʻolau volcano and juvenile tephra (Fig. 3). The Koko Rift tephra sequence is a classic locality for base-surge density currents (e.g., Fisher, 1977). The tephra locally has low angle cross bedding indicative of base surge explosions (Fig. 3). The tephra sequence is dominated by weak phreatomagmatic explosions that produced numerous dilute to concentrated pyroclastic surges (Rottas and Houghton, 2012).

3. Samples

The five largest subaerial flows along the Koko Rift were sampled (Fig. 2). They include Kalama, Kaupo (another large flow that extruded from a fissure in the cliff above a tourist destination, Sea Life Park), Koko Crater (at the NE margin of this largest tuff cone along the rift), the Lānaʻi Lookout (a narrow, ~600 m long flow that formed from a fissure on the southwest flank of Koko Crater), and the so-called Toilet Bowl (a narrow, ~700 m long flow that extruded from a fissure between the inner and outer rims of the Hanauma Bay tuff cone complex, another major tourist attraction). Two smaller flows (~2 m thick and ~ 10–15 m long) were also studied (Fig.1): One drapes the northeast wall of Hanauma Bay, and the other outcrops inside Nonoʻula crater and also high on the southwest wall of Hanauma Bay (Fig. 2). All of the flows were originally larger than shown on geologic maps (e.g., Stearns and Vaksvik, 1935). Much of the Koko Crater flow is buried by tephra and alluvium. The other flows are either partially underwater (Kaupo and Kalama), or terminated by marine erosion (Lānaʻi Lookout, Toilet Bowl and Hanauma Bay flows) and explosions (Nonoʻula). A lava sample was also collected on Kāohikaipu island, which is a separate eruptive center (Fig. 1). In addition, juvenile bombs were collected from Nonoʻula, Koko Crater and Mānana Island vent areas. Remnants of a coral reef produced during the marine sea level stage 5e higher stand of sea level (~5 m above current sea level at 114–130 ka; Szabo et al., 1994) underlie the tephra deposits at Lānaʻi Lookout. This reef was probably the primary source of the abundant coral reef fragments in the Koko tephra (Fig. 3) and provides a minimum age for Koko tephra deposits. These southern Koko Rift eruptions eventually built large subaerial cones and erupted four, small, late-stage lava flows (Stearns and Vaksvik, 1935).

We made two dredge hauls along the submarine section of Koko Rift while aboard the University of Hawaiʻi research vessel Moana Wave (Fig. 2). The deeper dredge (K1) on the eastern flank of a cone at water depths of 250–350 m in the middle of the submarine ridge collected tephra (including glassy spatter) and pillow lava. Dredge haul K2 on the west flank of the larger, shallow water cone (~100 m; Fig. 2) returned only coral debris.

Field evidence for the relative age of the Koko rift eruptions is scant. The path of the Kalama flow was apparently deflected by Koko Crater but tephra from Koko Crater locally overlies the Kalama flow (Winchell, 1947). Wentworth (1926) postulated significant time breaks between some of the Koko eruptions based on the presence of angular unconformities. However, no soil horizons separate any of the Koko Rift rock units and no apparent weathering occurred on any of the angular unconformity surfaces prior deposition of next tephra deposit. Thus, there were probably no significant time breaks between Koko Rift eruptions. Instead, the unconformities are probably related to migration of vent locations and local slumping during the eruptive sequence (Wentworth, 1951; Rottas and Houghton, 2012). The lava flows along the southern subaerial section (Lānaʻi Lookout to Nonoʻula Crater; Fig. 2) overlie the tephra. We concur with most previous studies (e.g., Winchell, 1947; Rottas and Houghton, 2012) that volcanism along the Koko Rift was probably coeval and may have occurred over weeks to a few months based on similar modern eruptions.

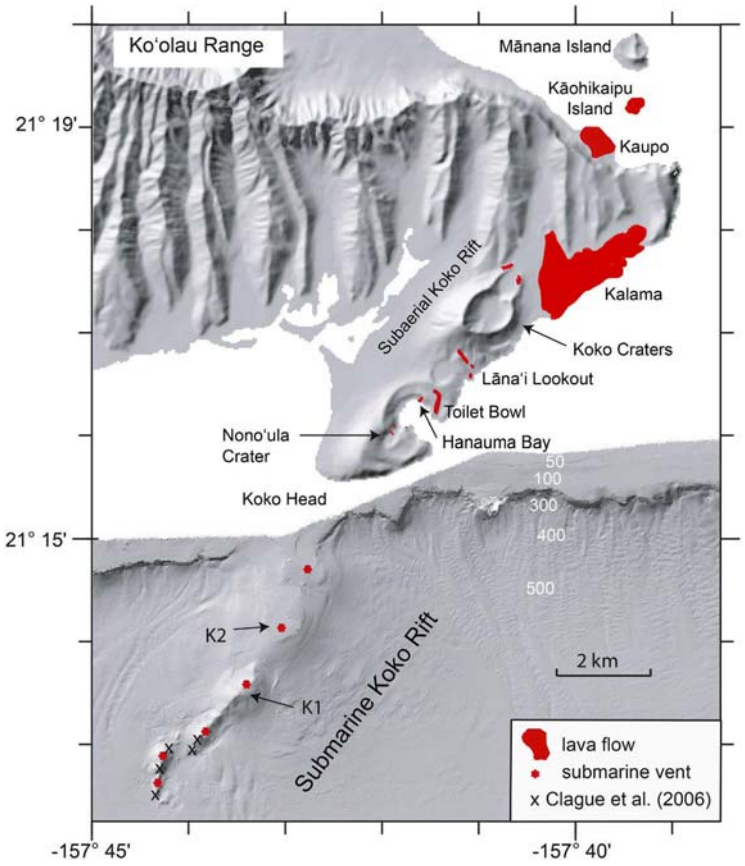

Fig. 2. Shaded relief map of the Koko Rift on southeast Oʻahu showing the location of vents and lavas flows (in red). The Rift is located on the eroded southern flank of Koʻolau volcano (2–3 Ma). K1 and K2 show locations and directions of dredge hauls on the submarine Koko Rift collected for this study. Basalt was recovered from dredge haul K1 but only coral was sampled from K2. The x's along the southern submarine ridge show locations where Clague et al. (2006) collected samples. The shaded relief image is from Dartnell and Gardner (1999). The white numbers in the area offshore from Hanauma Bay are depths in meters. (For interpretation of the references to colour in this figure legend, the reader is referred to the web version of this article.)

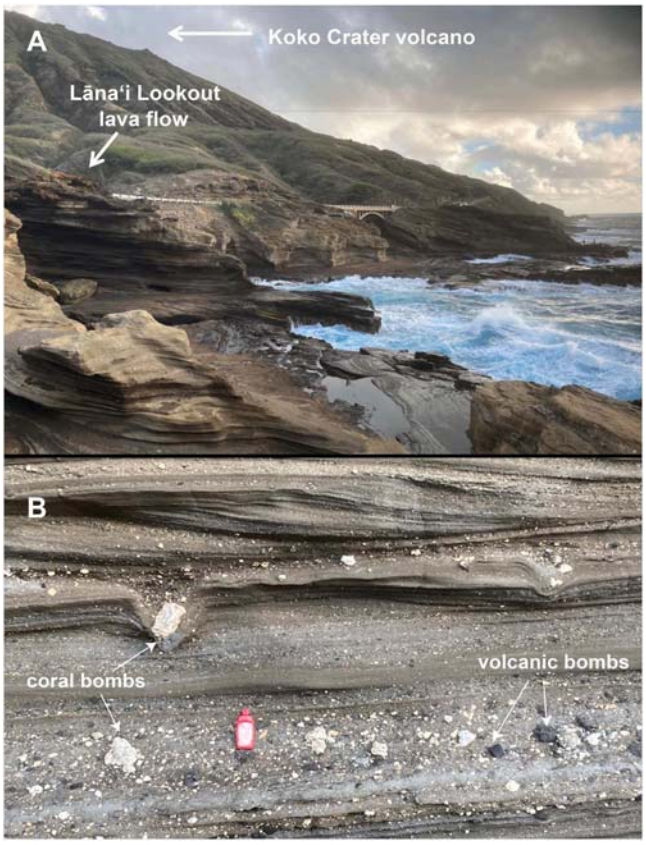

Fig. 3. Field photos of the Lāna'i Lookout area. A. Looking north with a lobe of the Lāna'i Lookout lava flow perched along a cliff and Koko Crater volcano is in the distance. B. Wave cut exposure into a tephra section. The lower layer has abundant blocks (white blocks are coral; dark blocks are mostly Ko'olau lava but some are juvenile bombs with breadcrust surfaces). Note the large coral block in the middle of the section with a pronounced bomb sag. Above the bomb sag are low-angle cross beds indicative of base surge activity. The red bottle is 19 cm tall. (For interpretation of the references to colour in this figure legend, the reader is referred to the web version of this article.)

Mānana Island (Fig. 1), which was considered by some studies as part of the Koko Rift (e.g., Wentworth, 1926; Winchell, 1947), formed by explosive eruptions. At the time Koko rift was erupting (~67 ka; Jicha et al., 2022), the Mānana Island area would have been ~30+ m above sea level and unlikely to have formed a tuff cone. Whereas Honolulu Volcanics tuff cones are thought to have been hydromagmatic involving trapped seawater in coral reefs (e.g., Macdonald et al., 1983). Also, the tephra from Mānana is petrographically and compositionally distinct from Koko Rift basalts with sparse needles of melilite (Wentworth, 1926) and rare hauyne microphenocrysts, and it has much lower SiO_2 compared to Koko Rift basalts (36–38 vs. 44–46 wt%; Clague and Frey, 1982). Thus, we concur with Macdonald et al. (1983) that the Mānana eruption was genetically unrelated to Koko Rift volcanism and probably formed at an earlier time when sea level was similar to today allowing interaction with seawater. Nonetheless, the petrologic features of the sample we collected from Mānana Island are discussed below because of its unusual nature and incomplete prior characterization.

4. Petrography

Petrographic observations were made on representative Koko Rift samples (Table 1). Most samples are olivine basalt (≥5 vol% total olivine), typically with sparse clinopyroxene (<2 vol%) and little or no plagioclase set in a glassy or cryptocrystalline matrix. Nepheline was reported in several Koko Rift flows (Winchell, 1947), although none was found in any of the samples we examined. Other studies have reported nepheline only in Honolulu Volcanic samples with 39.7–42.1 wt% SiO_2 (Clague and Frey, 1982), whereas all of our Koko Rift samples have >44.0 wt% SiO_2. The total abundance of olivine (phenocrysts, >0.5 mm across and microphenocrysts, 0.1–0.5 mm) varies greatly (0.2 vol% in the Toilet Bowl flow to 16.6 vol% in a Koko Crater flow; Table 1). In detail, there are two distinct petrographic populations of Koko Rift samples; those with ≥7 vol% total olivine and those with <3 vol% (Table 1). The submarine samples include both types of samples. Spinel inclusions are common in olivine.

Rare clinopyroxene (<0.1–2.0 vol%) phenocrysts or microphenocrysts are present in all but four subaerial samples. The K1 submarine basalts all have clinopyroxene but the abundance varies markedly (0.2–6.0 vol%; Table 1). Clinopyroxene occurs as crystal clots with olivine in the submarine samples and in one sample, as an oikocryst enclosing olivine. Plagioclase crystals larger than matrix size (>0.1 mm) are rare or absent (<1.5 vol%) in Koko Rift samples and, when present are almost always as microphenocrysts (Table 1). The samples collected at the distal southern end of the submarine ridge by Clague et al. (2006) (dive T273) are of two types, both with olivine microphenocrysts: samples from the deeper cone have plagioclase microphenocryts but lack clinopyroxene whereas samples from the other, slightly shallower and larger cone have clinopyroxene microphenocrysts similar to the samples from the K1 dredge haul.

The mineral abundance for multiple samples taken from the same flow or vent are similar, except for the Nono'ula blocks and the submarine flow (Table 1). The Kaupo and Kāohikaipu flows were thought to have erupted simultaneously and to be petrographically distinct from the nearby Kalama flow (Stearns and Vaksvik, 1935). However, the three Kalama flow samples we collected are petrographically similar to the Kaupo flow. The Kāohikaipu flow is distinct from the Kalama flow in having more plagioclase and clinopyroxene microphenocrysts (Table 1).

The Mānana Island bomb we examined has common olivine and rare clinopyroxene phenocrysts but is otherwise distinctive compared to Koko Rift samples. It contains rare hauyne microphenocrysts (1.0 vol%) and sparse melilite laths in the matrix but no plagioclase (Table 1). This is the second known occurrence of hauyne in Hawaiian basalts; the other is in the melilite nephelinite Mō'ili'ili flow (Winchell, 1947).

5. Mineral and glass chemistry

Olivine, clinopyroxene and plagioclase were analyzed in a several representative Koko Rift samples and one Mānana Island sample (Table 1). These are the first reported mineral analyzes of Koko Rift rocks. The Koko samples analyzed for mineral compositions span the full range of the Koko Rift rock compositions (e.g., 5.3–11.4 wt% MgO; Table 1). All analyzes were done at the University of Hawai'i using a five-spectrometer electron microprobe. Olivine and clinopyroxene were analyzed with beam conditions of 15 kV and 20 nA and a 3–5 μm wide beam. A lower current (10 nA) and a wider beam (10 μm) was used for analysis of hauyne and plagioclase to minimize sample degradation under the beam. Counting times were 30–60 s on the peak and 15 s on each side of the peak for the backgrounds. Na was measured in the first round of measurements to minimize its lost during analysis. No Na loss was detected in any of our mineral or glass analyses and the analysis totals are 99.0–100.5 wt%.

Olivine in Koko Rift samples show a complex history with both normal and reserve zoning (Figs. 4 and 5). Among the subaerial samples, core compositions range from forsterite (Fo) 78–85 in the higher MgO samples (>10 wt%) and Fo 78–82 in lower MgO rocks (<7 wt%; Table 2). One megacryst was found with Fo 88 and moderate CaO content (0.18 wt%; Table 2), indicating it is of crustal origin. CaO contents of the other Koko Rift olivine extend to high values (0.55 wt%; Table 2). The olivine in the submarine pillow lavas from Dredgehaul K1 and submersible collected samples T273-R6 and R9 are mostly either

Table 1
Petrography of representative Koko Rift rocks and a Manana Island bomb.

Sample (N to S)	MgO	Olivine		Clinopyroxene		Plagioclase		Matrix
Subaerial	wt%	ph	mph	ph	mph	ph	mph	
Mānana Island bomb^	13.6	3.2	4.6	0.2	<0.1	0.0	0.0	91.0
Kāohikaipu 2	11.4	6.6	4.8	<0.1	0.6	<0.1	1.2	86.8
Kaupo Flow	10.9	7.4	6.0	0.0	<0.1	0.0	0.2	86.4
Kaupo 4	10.8	7.0	6.4	0.0	<0.1	0.0	<0.1	86.4
Kalama 5	11.0	3.5	7.8	0.0	<0.1	0.0	<0.1	88.7
Koko Crater 3	10.9	3.8	4.0	1.2	1.8	0.0	0.0	89.2
Koko Crater bomb 1	11.2	8.6	3.8	0.0	<0.1	0.0	0.0	87.6
Lāna'i Lookout HV02–07	5.9	0.6	0.6	0.4	0.4	0.0	0.0	98.0
Toilet Bowl 1	5.3	0.2	0.0	0.4	0.4	0.0	0.2	98.8
Toilet Bowl HV02–08	5.2	0.0	0.6	0.0	0.2	<0.1	0.8	98.4
Hanauma Bay	6.1	0.4	0.4	0.0	0.0	0.0	0.4	98.8
Nono'ula	5.9	0.4	0.2	0.2	0.6	0.0	0.0	98.6
Nono'ula bomb 3	6.0	0.7	0.0	0.2	0.5	0.0	0.0	98.6
Nono'ula bomb 4	10.4	4.3	3.5	0.0	0.0	0.0	0.3	91.9
Submarine dredge haul K1								
K1–1	6.7	1.4	1.2	0.6	0.8	0.0	0.0	96.0
K1–5	9.1	4.2	1.0	4.2	0.2	0.0	0.0	90.4
K1–14	10.1	4.0	3.0	4.6	1.4	0.0	0.0	87.0
K1–18	5.8	0.4	0.2	<0.1	0.2	0.0	0.0	99.2
K1–33	10.0	5.0	3.4	0.2	<0.1	0.0	0.0	91.4
K1–38	9.3	2.4	1.4	0.4	0.2	0.0	0.0	95.6

Mode values are in volume % based on 500 counts/sample.
All samples are from flows except those listed as bombs.
Phenocrysts (ph) are >0.5 mm across; microphenocrysts (mph) are 0.1–0.5 mm across.
Matrix is glassy to cryptocrystalline with spinel, clinopyroxene, plagioclase and olivine.
^Contains 1.0 vol% hauyne mph and its matrix has melilite and nepheline but no plagioclase.
HV02 samples are from Ozawa et al. (2005).

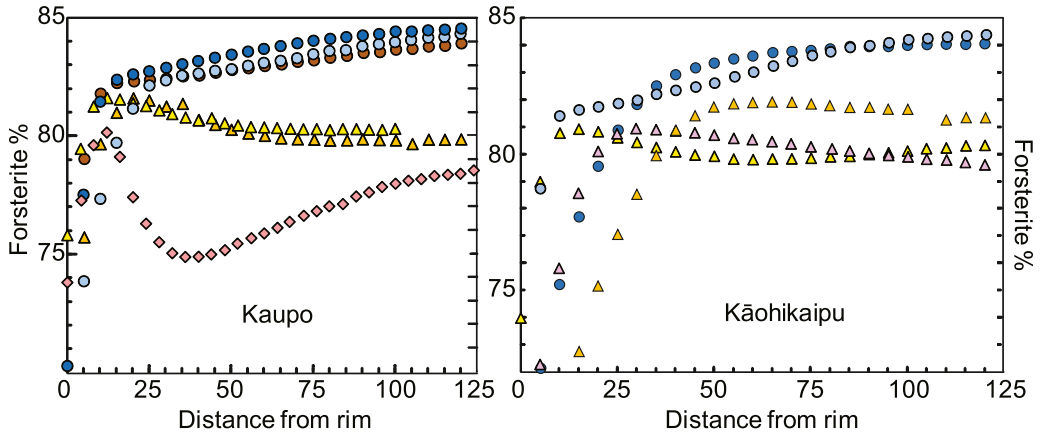

Fig. 4. Compositional zoning profiles for olivine in two, higher MgO Koko Rift subaerial lavas. The higher Fo olivine (84–85%) in both flows show normal but broad zoning with a sharp drop at 10–25 μm from the rim. The olivine with lower core Fo values (78–81%) show reverse zoning towards the rim indicating magma mixing.

unzoned or normally zoned but a few crystals from K1 have reverse zoning (Fig. 6). Core compositions range from Fo 80–82 in the K1 lavas with rims and microphenocryst cores at Fo 80–81 (Table 2). Olivine cores in the T273 samples range from Fo 81–84 (Table 2). The Fo content of the phenocryst cores in the higher MgO rocks (both subaerial and submarine) range from within the equilibrium field to Fo 2–5 units below (assuming a Fe/Mg K_d of 0.30; Roeder and Emslie, 1970). Olivine in the lower MgO subaerial rocks have Fo contents that overlap the equilibrium field to Fo 1–5 units too high. Thus, it would appear that the higher MgO rock compositions probably reflect both magma mixing and olivine accumulation. The Mānana Island bomb has higher Fo olivines (85–86) that are normally zoned (Table 2).

The clinopyroxene in the Koko Rift lavas record a complex magmatic history with both normal and reverse zoning in the submarine and subaerial lavas (Table 3; Fig. 6). Rocks from both areas have sector zoned clinopyroxene. Al_2O_3 compositions of these pyroxenes are highly variable; 3.3–6.2 wt% in the submarine rocks and 3.3–7.7 wt% in the subaerial rocks (Table 3). Generally, Al_2O_3 increases in steps towards the crystal margins. TiO_2 contents are moderate in all Koko Rift samples (0.9–2.9 wt%; Table 3).

Plagioclase is uncommon as a phenocryst or microphenocryst in Koko Rift volcanics (Table 1). Crystal cores have a narrow range in composition with anorthite (An) content (65–71) and low components of orthoclase (Or) (≤1.1), whereas rims vary greatly from An 71 to 42 with some crystals having higher An zones midway in their profiles (up to An 74; Table 4). The rim of one plagioclase with the lowest An content (42) has a higher Or (2.6). Normal and reverse An zoning (Table 4) were observed in both higher and lower MgO lavas.

Overall, the mineral zoning patterns and textures in these samples indicate that mixing occurred in the Koko Rift magmas (Figs. 4-6; Tables 2-4).

Hauyne was analyzed in a Mānana Island lava bomb (Table 5).

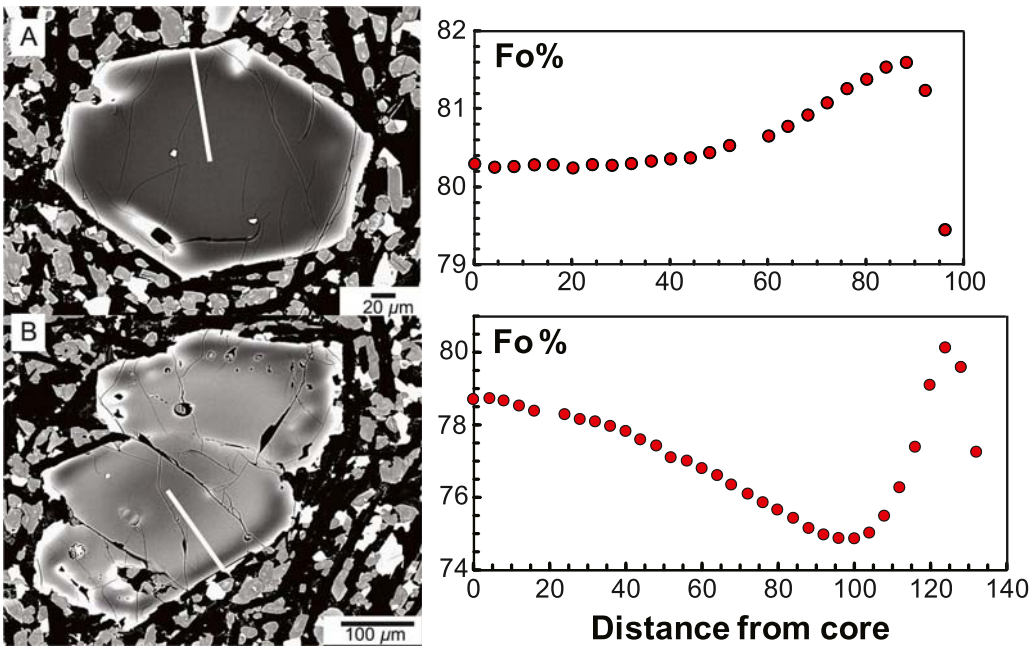

Fig. 5. Backscattered electron (BSE) images and forsterite (Fo%) zoning profiles of two olivines in the Kaupo flow. The intensity of the gray colour in the BSE images (A and B) reflects the average atomic number of the olivine (lighter colour for more iron-rich areas). Normally zoned crystals would have a dark (less Fe-rich) core and progressively get lighter towards their rim. A. Fo increases towards the crystal rim until the outermost ~10 μm, which is richer in iron. This is well documented in the compositional profile from the core to the rim (see white line) using a focused beam with 3 μm steps. B. Fo content gradually gets lower towards the rim until it abruptly increases (~5% Fo) ~40 μm from the rim. The Fo content decreased in the outer 10 μm of the crystal. These two crystals show that there is a mixed population of olivine in the Kaupo flow but that they both reacted to the influx of a more Mg rich melt. These profiles are representative of olivine in all of the Koko Rift flows that were analyzed, although reversely zoned crystals were more abundant in some samples.

Sodalite family minerals such as hauyne are extremely rare in Honolulu Volcanics rocks and were reported previously only in the Mōʻiliʻili melilite nephelinite flow (e.g., Winchell, 1947). Our new analyzes are the only ones available for sodalite family minerals in Hawaiian basalts. The Mānana Island hauyne crystals have a narrow compositional range with relatively high SO_3 (~10 wt%), CaO (~8.0 wt%) and Na_2O (14.3–16.3 wt%), and low Cl (0.4 wt%) and K_2O (0.9–1.2 wt%; Table 5). These values are similar to the analyzes for hauyne crystals from Colli Albani volcano in Italy, the classic hauyne locality in volcanic rocks (Conticelli et al., 2010). Typically, hauyne occurs in rocks with lower MgO, and more alkaline compositions (>10 wt%) and higher silica (40–45 wt%) than the Mānana Island basalt (Table 6).

Glass from a Mānana Island beach sand was analyzed by microprobe to compare with the whole rock composition. Low current (10 nA) and a wide beam (15 μm) was used to minimize Na loss. Analysis totals of 99.1–99.6 wt% for the 10 analyzed glasses indicate little or no Na loss during analysis. The glasses have a small range in composition with moderate MgO (5.0–5.4 wt%), high total alkali content of 9.6–10.7, and relatively high Cl content (0.23–0.30 wt%; Table S1). These compositions are similar to the Colli Albani (Italy) volcano rock compositions. However, the presence of hauyne in the Colli Albani rocks was related to assimilation of continental sedimentary rocks (e.g., Conticelli et al., 2010). No continental sediment is present in Hawaiʻi, so the presence of hauyne in the Mānana Island tephra was probably a primary magmatic feature.

6. Whole-rock XRF geochemistry

Our XRF analyzed samples span nearly the full length of the Koko Rift, and include all of its surface lava flows and bombs from several explosive centers (Fig. 2). Two samples were analyzed from several flows and seven from the submarine dredge haul K1. The XRF analyzes were made at the University of Massachusetts using methods described by Rhodes and Vollinger (2004) and their new Zeitum instrument. Three basaltic reference materials (BHVO-1, −2 and K1919; K1919 is an in-house recollection of the 1919 Kilauea flow that was sampled by the USGS for the BHVO reference materials) were analyzed with the Koko Rift samples as unknowns to check on data quality. The standard deviations about the mean value for the 7–12 analyses of these reference materials were low (<0.02 wt%, except for SiO_2 at 0.05 and 0.08 wt%), and our results for BHVO-1 and BHVO-2 compare well with those of Jochum et al. (2015) and for 25 other analyzes of K1919 run during 2021 (Table S2). Whole rock analyzes were previously reported for four subaerial Koko Rift flows (Kaupo, Kalama, Lānaʻi Lookout and Toilet Bowl) and five deep submarine lavas (T273) using a variety of methods in different labs spanning six decades (Winchell, 1947; Jackson and Wright, 1970; Clague and Frey, 1982; Clague et al., 2006; Fekiakova et al., 2007). Here we compare the new Koko Rift XRF results with data collected from the same lab for other Honolulu Volcanics eruptions (Fig. 7).

The Koko Rift samples are weakly alkalic basalts with moderate SiO_2 (44–46 wt%) and total alkali contents (3.3–5.2 wt%), and a wide MgO range (5.2–11.4 wt% MgO; Table 6) including the lowest MgO values among Honolulu Volcanics (Fig. 7). The higher MgO Koko samples (9–11 wt%; red triangles) have relatively low incompatible major (Ti, K and P) and trace element abundances compared to analyses for other Honolulu Volcanics rocks (e.g., Nb, 22–38 ppm; Sr, 580–1021 ppm; Fig. 7). The compatible trace elements (Ni and Cr) are moderate in concentration in the higher MgO samples (192–277 ppm Ni, 384–488 ppm Cr; Table 6). The two northernmost Koko Rift flows, Kāohikaupu and Kaupo (pink triangles), and three of the submarine samples (purple triangles) collected by Clague et al. (2006) from a cone near the southern end of the Koko Rift have lower TiO_2 and incompatible element (Nb, Sr and Zr) contents compared to the other Koko basalts with similar MgO contents (Fig. 7). These differences indicate these rocks from opposite ends of the rift zone were probably derived from compositionally similar

Table 2
Representative microprobe analyses of olivines in Koko Rift and Manana Island rocks.

Sample	T273-R6				T273-R9			
Rock Mg#	63.9				64.2			
Size	ph-c	ph-c	ph-c	ph-c	ph-c	ph-c	ph-c	ph-c
SiO_2	39.81	39.88	39.24	39.68	39.95	40.03	39.4	39.06
FeO	15.01	15.03	16.56	16.49	15.13	15.28	17.16	17.54
MnO	0.18	0.19	0.23	0.22	0.21	0.21	0.26	0.26
MgO	45.04	44.82	43.84	43.22	44.29	44.15	42.52	42.22
CaO	0.26	0.25	0.29	0.3	0.27	0.28	0.39	0.36
Total	100.3	100.2	100.2	99.91	99.85	99.95	99.73	99.44
Fo %	84.4	84.2	82.7	82.4	83.9	83.7	81.6	81.1

Sample	K1–33				K1–38				Nonoula flow			
Rock Mg#	61.0				57.1				49.9			
Size	ph-c	ph-r	ph-c	ph-r	ph-c	ph-r	mph-c	mph-r	mph-c	mph-r	ph-c	ph-r
SiO_2	39.16	38.93	39.8	39.56	39.75	39.3	38.96	39.16	39.32	39.32	39.64	38.51
FeO	16.16	17.82	16.51	17.9	15.14	17.72	18.06	18.06	18.55	19.23	16.84	16.60
NiO	0.25	0.19	0.20	0.20	0.28	0.18	0.21	0.28	0.17	0.15	0.20	0.18
MgO	43.75	42.40	43.24	42.02	44.84	42.28	42.33	42.15	41.58	40.74	43.04	43.05
CaO	0.25	0.34	0.30	0.44	0.26	0.40	0.40	0.43	0.38	0.42	0.40	0.48
Total	99.57	99.69	100.05	100.12	100.27	99.88	99.96	100.08	100.00	99.86	100.12	99.82
Fo%	82.8	80.9	82.3	80.7	84.0	81.0	80.6	80.6	80.0	79.1	82.0	82.2

Sample	Toilet Bowl HV02–08		Hanauma Bay		Koko Crater bomb 1				Koko Crater flow 3			
Rock Mg#	47.0		49.6		64.1				63.5			
Size	ph-c	ph-r	mph-c	mph-c	ph-c	ph-r	mega-c	mega-r	ph-c	ph-r	ph-c	ph-r
SiO_2	39.12	39.1	38.25	39.11	39.71	39.90	41.01	39.55	39.47	37.61	39.71	38.45
FeO	20.19	20.52	20.47	16.91	16.52	15.63	10.99	16.76	15.56	25.48	16.56	22.37
NiO	0.17	0.15	0.10	0.14	0.23	0.27	0.51	0.19	0.30	0.12	0.16	0.10
MgO	40.27	39.94	40.38	43.30	43.26	43.75	47.75	42.94	44.08	35.34	43.37	38.07
CaO	0.41	0.43	0.40	0.31	0.31	0.28	0.22	0.42	0.20	0.55	0.25	0.47
Total	100.2	100.1	99.67	99.84	100.03	99.83	100.48	99.86	99.57	99.29	100.05	99.46
Fo%	78.0	77.6	77.9	82.0	82.4	83.4	88.6	82.0	84.3	76.4	82.4	75.2

Sample	Kaupo flow 1				Kāohikaipu Island 2				Mānana bomb 1			
Rock Mg#	63.9				64.6				67.5			
Size	ph-c	ph-r	ph-c	ph-r	ph-c	ph-r	mph-c	mph-r	ph-c	ph-r	mph-c	mph-r
SiO_2	39.56	38.36	39.06	38.81	39.75	38.49	39.80	39.43.	40.07	39.57	40.13	39.65
FeO	14.93	22.17	17.04	19.17	15.41	21.11	16.08	18.86	13.44	15.30	14.15	15.61
NiO	0.32	0.19	0.20	0.18	0.19	0.16	0.19	0.16	0.28	0.09	0.23	0.12
MgO	44.44	38.28	42.60	40.74	44.35	39.85	43.73	41.00	46.44	44.63	45.70	44.56
CaO	0.26	0.35	0.32	0.37	0.35	0.40	0.26	0.38	0.20	0.55	0.23	0.49
Total	99.52	99.36	99.23	99.28	100.05	100.01	100.06	99.83	100.42	100.14	100.44	100.43
Fo %	84.1	75.5	81.7	79.1	83.7	77.1	82.9	79.4	86.1	83.8	85.2	83.6

Rock Mg #-whole rock [Mg/(Fe^{2+} +Mg)] x 100 with Fe^{2+} = 0.9 total iron.
ph- phenocryst; mph- microphenocry; c-core; r-rim; mega- megacryst.
Fo (forsterite) one sigma error ± 0.25% Fo based on counting statistics.

parental magmas. The K1 submarine lavas (blue triangles) show a remarkable range and linear trends in most major and trace element abundances (e.g., 5.8–10.0 wt% MgO). In contrast, the two submarine samples collected from deepest and southernmost Koko Rift cone have the highest MgO (~12.7 wt%) among Koko Rift lavas but otherwise are similar in composition and lie along linear trends with subaerial Koko Rift samples (Table 6, Fig. 7). Overall, the Koko Rift basalts are compositionally unusual among Honolulu Volcanics basalts.

The Mānana Island sample was only analyzed by XRF for major elements because of its small size. It has low SiO_2 (39 wt%) and TiO_2 (2.0 wt.) and high MgO (13.6 wt%; Table 6), similar to other nephelinites from the Honolulu Volcanics (Fig. 7).

7. ICPMS trace elements

Five Koko Rift samples and the Mānana Island bomb were analyzed by ICPMS (Table 7) using methods described in Garcia et al. (2021) at the University of Tasmania and Research School of Earth Sciences at the Australian National University in three sessions during 1999–2002. The reference material BHVO-1 was used for calibration of element sensitivities with several USGS and in-house basaltic reference materials analyzed to document accuracy and precision of the method (Table S3). These new data are plotted along with published ICMPS analyzes for 10 other Koko Rift samples from Yang et al. (2003), Clague et al. (2006) and Fekiakova et al. (2007) after examining their results for known reference materials. The Yang et al. (2003) data were corrected to USGS reference basalt BHVO-2 based on our previous data as presented in Garcia et al.

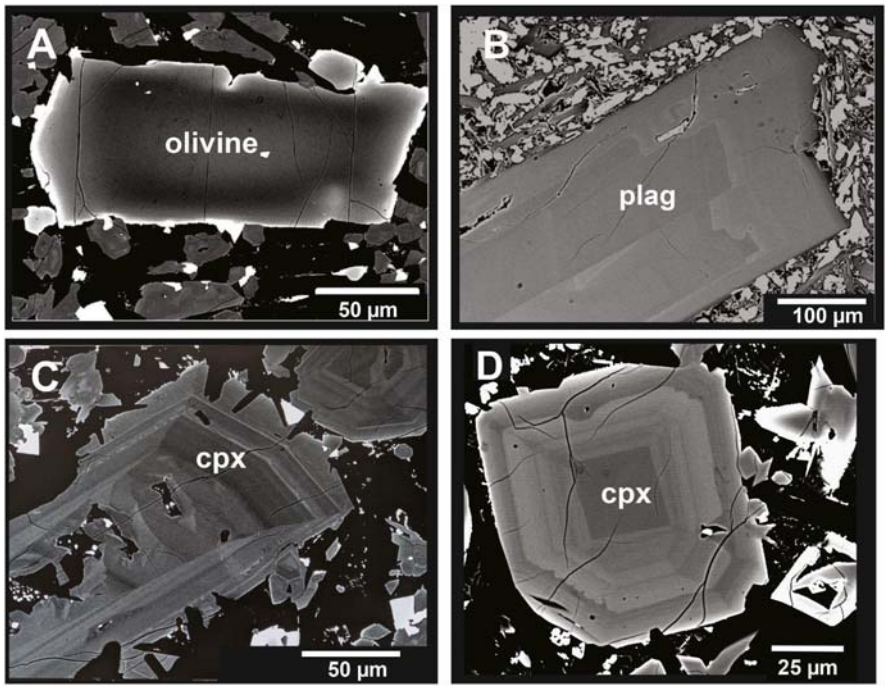

Fig. 6. Backscattered electron images of minerals in Koko Rift lavas. A. Olivine from a submarine basalt flow, K1–33, showing composition zoning. The crystal core is richer in iron (lighter gray); the intermediate part of the crystal is darker and more Mg-rich. The rim is the most iron-rich part of the crystal. B. Plagioclase (plag) from the Hanauma Bay flow showing multiple zones of higher anorthite content (dark areas) including at the outer rim. C. Complexly zoned clinopyroxenes (cpx) from the Toilet Bowl flow with multiple Mg-richer and Fe-richer zones. D. Complexly zoned cpx from the submarine basalt K1–33. The outer dark zone shows a ragged inner edge indicating dissolution before the Mg-rich (darker) overgrowth.

Table 3
Representative microprobe analyses of clinopyroxenes in Koko rift lavas.

Sample	K1–14				K1–33				Nono'ula flow				Hanauma Bay		
Size	ph-c	ph-r	ph-c	ph-r	ph-c	ph-r	ph-c	ph-r	mph-c	mph-r	mph-c	mph-r	mph-c	mph-c	mph-r
SiO_2	49.92	48.5	51.03	48.14	50.2	49.6	48.96	48.96	49.97	48.1	48.88	50.04	46.43	50.15	46.32
TiO_2	1.06	1.26	1.10	1.95	1.08	1.25	1.29	1.39	1.08	1.95	1.58	1.15	2.33	1.11	2.27
Al_2O_3	4.12	5.52	3.43	6.84	3.91	4.16	4.92	5.50	3.65	5.97	3.80	3.45	6.89	3.59	6.79
Cr_2O_3	0.43	0.79	0.69	0.31	0.65	0.69	0.91	0.74	0.28	0.51	0.20	0.26	0.13	0.29	0.20
FeO	6.04	6.16	5.94	7.06	5.79	5.97	5.85	6.25	6.20	6.67	8.10	6.13	7.52	6.06	7.53
MgO	15.16	14.3	15.09	13.35	14.97	14.6	14.20	13.85	14.99	13.38	13.84	14.9	12.69	14.93	12.93
CaO	22.25	22.3	22.49	22.15	22.8	23.01	23.16	22.90	22.62	22.99	22.37	22.9	22.93	23.26	23.04
Na_2O	0.43	0.52	0.34	0.43	0.39	0.33	0.41	0.43	0.35	0.37	0.39	0.32	0.40	0.35	0.42
Total	99.41	99.29	100.11	100.23	99.84	99.60	99.70	100.02	99.14	99.91	99.16	99.20	99.32	99.74	99.50
En	43.9	42.4	46.7	48.3	43.2	42.4	41.6	40.9	43.2	39.8	40.2	42.8	38.0	42.6	38.4
Fs	9.8	10.2	9.6	11.5	9.4	9.7	9.6	10.4	10.0	11.1	13.2	9.9	12.6	9.7	12.5
Wo	46.3	47.4	43.6	40.2	47.4	47.9	48.8	48.7	46.8	49.1	46.6	47.3	49.4	47.7	49.1

Sample	Lāna'i Lookout HV02–07				Toilet Bowl HV02–08				Koko Crater flow 3				Kāohikaipu 2			
Size	ph-c	ph-r	ph-c	ph-r	ph-c	ph-r	ph-c	ph-r	ph-c	ph-r	ph-c	ph-r	mph-c	mph-r	mph-c	mph-r
SiO_2	50.59	46.03	50.36	47.58	50.35	49.25	48.11	47.20	44.72	49.12	50.34	49.44	50.16	50.38	50.17	46.59
TiO_2	0.86	2.73	1.09	1.90	1.11	1.53	1.51	2.65	2.88	1.48	1.14	1.44	1.11	1.12	1.11	2.27
Al_2O_3	3.91	7.09	3.60	6.17	3.69	4.34	7.90	7.67	7.69	3.92	3.30	4.24	3.36	3.40	3.37	6.97
Cr_2O_3	0.61	0.17	0.31	0.45	0.28	0.07	0.06	0.11	0.07	0.20	0.48	0.08	0.33	0.25	0.26	0.38
FeO	5.95	7.86	6.08	6.91	6.15	7.30	7.69	7.83	8.67	6.99	5.70	7.05	6.75	6.73	6.97	8.09
MgO	15.40	12.39	14.86	13.30	14.78	14.03	12.44	12.28	11.85	14.46	14.95	14.25	15.13	15.10	15.03	12.48
CaO	22.22	22.81	23.25	23.05	23.13	22.81	0.44	0.47	22.69	22.79	23.15	22.96	22.33	22.53	22.33	22.13
Na_2O	0.46	0.43	0.35	0.41	0.36	0.33	22.18	22.01	0.46	0.29	0.34	0.34	0.30	0.31	0.27	0.44
Total	100.00	99.51	99.90	99.77	99.85	99.66	100.32	100.23	99.03	99.25	99.40	99.80	99.47	99.82	99.51	99.35
En	44.4	37.3	42.5	39.4	42.4	40.6	48.8	48.7	35.9	41.6	43.0	41.0	43.3	43.0	43.0	37.9
Fs	9.6	13.3	9.8	11.5	9.9	11.9	38.1	37.8	14.7	11.3	9.2	11.4	10.8	10.8	11.1	13.8
Wo	46.0	49.4	47.7	49.1	47.7	47.5	13.2	13.5	49.4	47.1	47.8	47.6	45.9	46.2	45.9	48.3

ph-phenocryst; mph-microphenocryst; c-core; r-rim.
One sigma error based on counting statistics: En (enstatite); ± 0.10% Fs (ferrosilite) ± 0.18%; Wo (wollastonite) ± 0.05%.

(2021).

The Koko Rift samples range widely in Th abundances (0.9–3.5 ppm) and La/Yb ratios (0.9–19.9; Fig. 8). In plots of La/Yb and Zr/Nb vs. Ba/Th, the submarine samples (purple diamonds and blue triangles) form endmembers (Fig. 8). The subaerial lavas have intermediate compositions on these ratio-ratio plots (Fig. 8).

Table 4
Representative microprobe analyses of plagioclase in Koko Rift rocks.

Sample	Toilet Bowl HV02–08						Lānai Lookout HV02–07				
	ph-c	ph-mid	ph-r	ph-c	ph-mid	ph-r	ph-c	ph-r	ph-c	ph-mid	ph-r
SiO_2	50.34	51.01	50.16	50.00	49.59	51.36	51.20	50.20	51.61	50.91	56.71
Al_2O_3	31.23	30.65	31.07	31.49	31.75	30.58	30.87	31.3	30.50	30.85	27.12
FeO	0.61	0.63	0.85	0.52	0.64	0.74	0.53	0.60	0.87	0.68	0.40
CaO	3.24	3.77	3.40	3.27	3.01	3.82	13.72	14.2	3.91	3.57	6.30
Na_2O	14.18	13.47	13.83	14.30	14.46	13.20	3.46	3.21	13.27	13.73	8.80
K_2O	0.13	0.17	0.15	0.14	0.12	0.18	0.14	0.09	0.18	0.16	0.45
Total	99.80	99.79	99.53	99.80	99.63	99.96	99.92	99.60	100.45	100.00	99.79
An %	70.2	65.7	68.6	70.1	72.1	65.0	68.4	70.7	64.6	67.4	42.4
Or %	0.8	1.0	0.9	0.8	0.7	1.0	0.8	0.6	1.1	1.0	2.6

Sample	Hanauma Bay 1						Kāohikaipu 2			
	ph-c	ph-mid	ph-r	mph-c	mph-mid	mph-r	mph-c	mph-r	mph-c	mph-r
SiO_2	50.23	49.16	51.73	50.55	49.56	50.57	50.35	52.2	50.75	50.33
Al_2O_3	31.32	32.18	30.42	31.48	31.83	30.89	30.93	29.6	31.19	31.55
FeO	0.66	0.63	0.80	0.66	0.68	0.74	0.57	1.00	0.63	0.64
CaO	3.29	2.91	3.89	3.31	2.97	3.61	13.76	12.1	14.35	14.48
Na_2O	14.30	15.06	13.18	14.03	14.67	13.94	3.44	4.19	3.35	3.16
K_2O	0.12	0.11	0.20	0.13	0.12	0.15	0.12	0.20	0.10	0.11
Total	100.01	100.13	100.22	100.16	99.87	99.99	99.17	99.2	100.37	100.27
An %	70.1	73.6	64.4	69.5	72.7	67.5	68.9	61.3	70.0	71.5
Or %	0.7	0.7	1.2	0.8	0.7	0.9	0.7	1.2	0.6	0.7

ph- phenocryst; mph- microphenocry; c-core; r-rim; mid- middle of crystal.
An %- anorthite compoent; Or %- orthoclase component.
± 0.25% An based on counting statistics.

Table 5
Microprobe analyses of hauyne in a Mānana Island bomb.

Size	ph-c	ph-r	mph-c	mph-r
SiO_2	33.76	32.81	33.92	33.97
Al_2O_3	30.15	29.48	30.58	30.05
FeO	0.36	0.43	0.41	0.50
MgO	0.35	0.32	0.35	0.33
CaO	8.29	7.83	8.03	8.24
Na_2O	15.21	16.33	14.26	14.35
K_2O	1.02	1.24	0.94	0.96
Cl	0.72	0.73	0.70	0.64
SO_3	9.84	10.12	10.07	10.44
Total	99.70	99.29	99.26	99.48

The Mānana Island basalt ICPMS results are consistent with the XRF data showing this nephelinitic basalt is highly enriched in incompatible elements (Table 7) like other Honolulu Volcanics nephelinites (Yang et al., 2003; Fekiakova et al., 2007). The Mānana basalt has 2–3 times higher abundances for most highly incompatible elements compared to Koko Rift sample (e.g., Th 9.4 vs. 3.6 ppm; La 78 vs. 33; Table 7). Likewise, the Mānana sample has higher ratios of La/Yb, double the value for any Koko Rift basalt (44 vs. <20). Thus, the results for the Mānana Island basalt are not plotted on Fig. 8 because they would reduce the resolution of trace element variation among Koko Rift samples.

8. Discussion

8.1. Magma mixing and crystal fractionation

Koko Rift basalts show ample mineralogical evidence of magma mixing (Figs. 4-6 and Tables 2-5). No previous study of Honolulu Volcanics reported evidence of magma mixing and we found none for the Mānana Island sample. Clague (1987) argued that Hawaiian rejuvenation-stage magmas ascended rapidly to the surface from depths of ~100 km or more without storage in crustal magma chambers based on their high MgO contents (e.g., 10.6–14.4 wt%; Fig. 7) and the common occurrence of mantle xenoliths (usually spinel peridotite but in some cases garnet-bearing peridotite and pyroxenite; e.g., Sen et al., 2005) in Honolulu Volcanics deposits. Ascent rates of 0.2–25 ms^{-1} were estimated using H diffusion in olivine from mantle xenoliths in the Honolulu Volcanics Salt Lake Crater (SLC) deposit (Peslier et al., 2015). At these rates, it would have taken less than a day for magma to rise to the surface from mantle depths where SLC garnet pyroxenite xenoliths were inferred to have been entrained (~45–55 km; Guest et al., 2020). No mantle xenoliths have been found in Koko basalts unlike deposits from most Honolulu Volcanics eruptions (e.g., Sen et al., 2005). The moderate forsterite and NiO contents of the olivine cores (Fo 82–85, NiO 0.19–0.30 wt%; Table 2) in the higher MgO (10.1–11.4 wt%) Koko Rift lavas indicate they underwent crystal fractionation and are not near primary mantle melts. The presence of four strongly fractionated (5.2–6.1 wt. MgO and < 100 ppm Ni; Table 6, Fig. 7) basalts along the southern subaerial rift section also demonstrate significant crystal fractionation, probably within the crust prior to eruption. These lower MgO samples are unique among the Honolulu lavas (Fig. 7). Taken together, the mineral and whole rock results for the Koko Rift rocks indicate magma was stored in the crust and underwent variable amounts of crystal fractionation and accumulation before being mixed prior to eruption.

Modeling of incompatible trace element abundances and ratios indicated three magmas were apparently involved in the Koko Rift magmatism. Plots of La/Yb vs. Th, and Ba/Th vs. Zr/Nb and La/Yb show that the basalt compositions from the southernmost submarine cone (3 purple diamonds in Fig. 8) with high Ba/Th but low La/Yb could have mixed with the composition of the submarine K1 basalts (light blue triangles) to generate much of the wide range in trace element ratios observed for the subaerial Koko Rift samples (Fig. 8). Basalt from the southernmost cone shows no evidence of magma mixing based on our microprobe examination of its olivine and plagioclase (Fig. S2). Some of the scatter in the ratio plots may be related to mixing with the basalt composition from the cone just north of the southern cone (two purple diamonds in Fig. 8). However, our examination of basalt from this cone shows it experienced magma mixing based on backscattered images of clinopyroxene that show compositional reversals (Fig. S3). Thus, nearly

Table 6
XRF results for Koko Rift samples. Fe_2O_3* is total iron.

Location	Submarine								Nono'ula		
	K1–01	K1–05	K1–14	K1–18	K1–22	K1–33	K1–35	K1–38	flow	bomb 3	bomb 4
SiO_2	45.76	45.24	44.98	46.11	44.721	45.08	45.95	45.74	46.39	46.48	44.83
TiO_2	2.41	2.22	2.20	2.45	2.335	2.16	2.33	2.332	2.40	2.38	2.21
Al_2O_3	14.72	13.57	12.96	15.05	13.38	13.00	14.24	13.95	15.00	15.04	12.74
Fe_2O_3*	13.19	13.55	13.72	13.42	13.99	13.72	13.27	13.23	13.04	13.25	13.98
MnO	0.18	0.180	0.19	0.18	0.19	0.19	0.19	0.19	0.19	0.18	0.19
MgO	6.66	9.14	10.14	5.84	9.34	10.02	7.54	8.02	5.89	6.00	10.43
CaO	11.71	11.11	11.42	11.73	12.35	11.26	11.58	11.89	11.58	11.63	10.85
Na_2O	3.67	3.47	3.04	3.86	2.77	3.20	3.28	2.99	3.60	3.56	3.24
K_2O	1.00	0.92	0.76	1.06	0.66	0.89	0.82	0.84	0.99	0.97	0.92
P_2O_5	0.60	0.55	0.50	0.60	0.48	0.53	0.55	0.58	0.60	0.57	0.50
Total	99.89	99.95	99.91	100.31	100.21	100.06	99.75	99.74	99.68	100.06	99.89
LOI	0.44	0.63	1.45	0.03	2.74	0.89	0.54	2.06	0.53	0.47	0.45
Nb	37.8	34.4	33.9	38.9	35.4	33.2		37.7	35.6	35.4	35.5
Rb	23.0	21.2	21.1	24.9	13.6	20.9		26.3	23.7	23.6	22.7
Ba			489	563		514		554	549	582	594
Nb	37.8	34.4	33.9	38.9	35.4	33.2		37.7	35.6	35.4	35.5
Zr	144	132	129	148	133	128		149	141	141	131
Y	24.7	22.6	20.8	25.3	20.4	21.7		28.1	25.4	24.8	21.5
Sr	897	798	871	913	962	815		893	931	885	761
Zn	132	132	140	129	127	131		130	129	133	134
Ni	95	165	186	61	145	193		163	65	67	238
Cr	202	327	365	109	319	394		329	82	113	407
V	274	250	253	269	261	244		267	282	276	252

Hanauma Bay	Toilet Bowl		Lāna'i Lookout	Koko Crater		Kalama flow		Kaupo flow		Kāohi-kaipu 2	Mānana
	HV 02–08	1	HV 02–07	bomb 1	flow 3	1	5	1	4		
46.25	46.34	46.23	46.36	44.28	44.83	44.51	44.36	45.41	45.33	45.57	38.91
2.37	2.46	2.44	2.40	2.19	2.24	2.26	2.30	1.99	2.02	1.91	2.00
15.04	15.51	15.57	14.97	12.31	12.39	12.40	12.29	13.07	13.14	13.28	11.63
13.31	13.31	13.52	13.15	13.98	13.78	14.03	14.35	13.62	13.82	13.90	14.44
0.18	0.20	0.19	0.19	0.19	0.20	0.19	0.19	0.19	0.18	0.18	0.24
6.11	5.18	5.33	5.91	11.17	10.92	10.85	11.05	10.94	10.84	11.40	13.61
11.62	11.10	11.18	11.34	11.18	10.80	10.94	10.92	10.54	10.61	10.51	11.26
3.54	4.14	3.88	3.96	3.17	3.39	3.28	3.22	3.02	3.00	2.67	5.02
1.05	1.02	1.02	0.98	0.95	0.92	0.78	0.75	0.74	0.74	0.64	1.18
0.58	0.63	0.61	0.58	0.49	0.48	0.63	0.46	0.42	0.38	0.32	1.31
100.05	99.88	99.97	99.84	99.90	99.96	99.88	100.10	99.95	100.06	100.38	99.61
1.99	−0.49	0.25	−0.43	0.77	0.55	−0.11	−0.05	−0.47	−0.26	0.88	0.65
34.7	37.2	37.0	35.9	33.9	35.8	35.0	33.3	23.8	23.9	21.8	
25.3	25.5	25.3	24.7	22.4	23.2	16.8	22.4	18.2	16.4	10.7	
601	623	674	589	416	523	493	496	383	381	323	
34.7	37.2	37.0	35.9	33.9	35.8	35.0	33.3	23.8	23.9	21.8	
137	144	145	143	129	132	135	134	104	105	97	
24.6	26.6	26.2	24.5	20.2	21.4	21.1	21.3	19.2	19.6	18.4	
915	1032	1021	877	717	725	741	733	611	616	586	
121	132	130	127	128	118	129	115	116	116	117	
68	55	54	73	258	261	256	242	275	274	279	
96	112	115	111	461	472	457	419	476	466	432	
257	281	277	277	247	281	258	260	240	238	243	

all of the Koko Rift basalts experienced magma mixing to varying degrees with compositions similar to the submarine samples forming endmembers (Fig. 8).

The lower MgO (5.2–6.1 wt%) subaerial lavas were erupted near the end of Koko Rift volcanism based on their stratigraphic positions as surface or near surface flows on the southern tuff cones. However, there is no apparent time gap between their eruption and the underlying tephra based on the absence of a weathering horizon under the flows. Two crustal magmatic processes affected these Koko lavas: crystal fractionation followed by magma mixing. Their low MgO, unique among Honolulu Volcanics, indicates these lavas underwent significant crystal fractionation prior to eruption. Fractionation was followed by mixing with more Mg-rich magma based on the reverse zoning on the rims of the minerals in these rocks (Fig. 6, Tables 2 and 4). This mixing event may have triggered their eruption.

8.2. The Koko Rift mantle source

Honolulu basalts have a restricted range in Pb, Sr and Nd but a wide range in trace element compositions (e.g., Clague and Frey, 1982; Stille et al., 1983; Lassiter et al., 2000; Yang et al., 2003; Clague et al., 2006; Fekiakova et al., 2007). Most of these basalts have high MgO (10–16 wt %), which led to modeling of their trace element variation by variable degrees of melting (e.g., Clague and Frey, 1982; Yang et al., 2003). The Koko basalts also have a limited range in Sr, Nd and Pb isotopes ($^{87}Sr/^{86}Sr$ = 0.7033–0.7035; ε_{Nd} = +7.6–8.1; $^{206}Pb/^{204}Pb$ = 18.09–18.15; $^{207}Pb/^{204}Pb$ = 15.43–15.46; $^{208}Pb/^{204}Pb$ = 37.71–37.81; Lassiter et al., 2000; Clague et al., 2006; Fekiakova et al., 2007). Although the wide range of trace element compositions among the higher MgO (9–12.7 wt%) Koko basalts (e.g., Th 0.9–3.5 ppm, La/Yb = 9–20) might be interpreted as reflecting variable degrees of partial melting of a single source (implied by the relatively constant isotopic compositions) the large ranges in ratios of Ba/Th (156–264), two highly

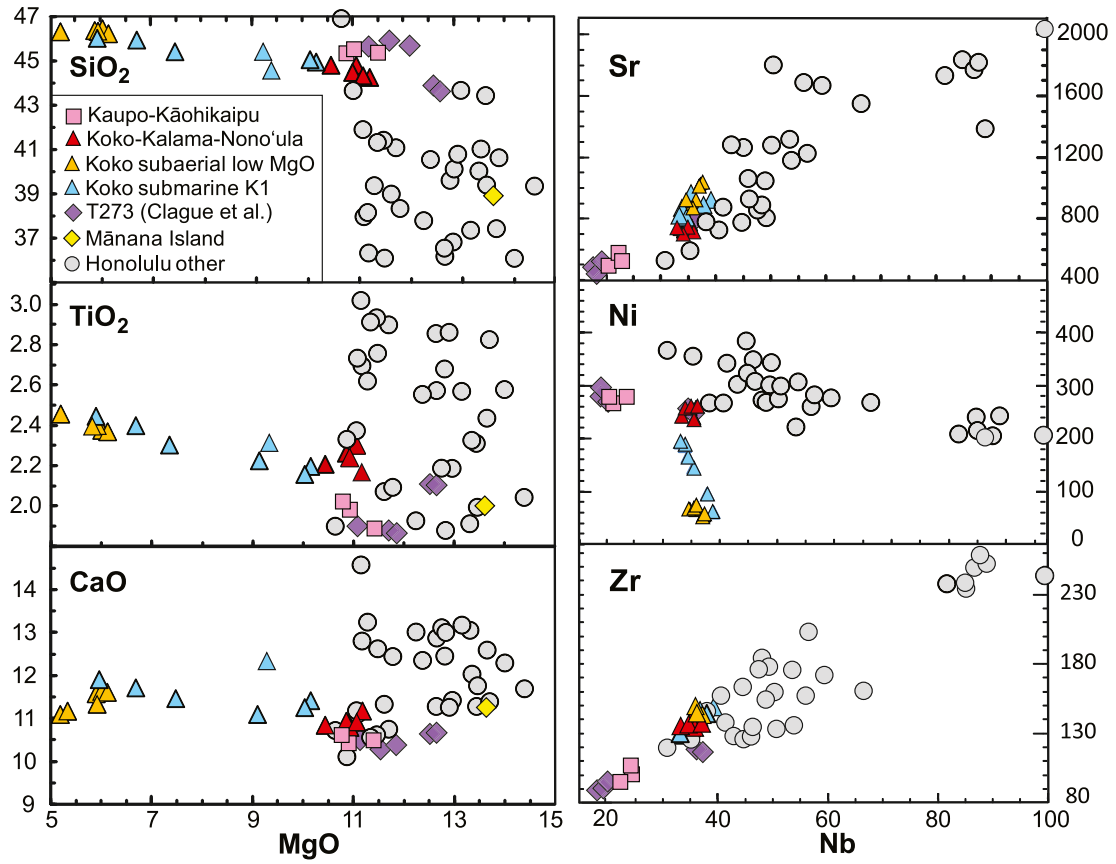

Fig. 7. Plots of XRF whole-rock major and trace element data for Koko Rift (triangles) and one Mānana Island basalt (yellow diamond; see Table 6 for the data) compared to other Honolulu Volcanics basalts analyzed in the same lab (gray circles). The Koko Rift basalts are atypical in their relatively high SiO_2 and diverse MgO abundances. (For interpretation of the references to colour in this figure legend, the reader is referred to the web version of this article.)

incompatible elements, require a heterogeneous source. The effects of metasomatic enrichment, partial melting and residual phases on compositions of Koko Rift lavas are difficult to disentangle. For example, the positive Ba anomalies that are apparent on normalized trace element patterns of Koko lavas (Clague et al., 2006) may be due either to source enrichments or a metasomatic residual phase such as phlogopite (Yang et al., 2003).

Geochemical characteristics expected for involvement of residual phlogopite in the Koko source can be evaluated based on experimentally determined partition coefficients. Literature data for the alkali and alkaline earth elements in phlogopite vary over about an order of magnitude and depend on the composition of the phlogopite. General characteristics of element partitioning in phlogopite are Rb > Ba>Cs and Sr > Nd (e.g., LaTourrette et al., 1995; Schmidt et al., 1999; Krmíček et al., 2014). Thus, residual phlogopite would be expected to produce magmas with low Rb/Cs, high Ba/Rb, and low Sr/Nd. Although the Koko lavas have Ba/Rb ratios greater than typical for ocean island basalts (16–51, avg. 25 vs. 12.5; Hofmann and White, 1983), they also have Rb/Cs ratios similar to average OIB (71–194, avg. 97 vs. 106; Hofmann and White, 1983) and Sr/Nd ratios similar to or greater than those of the Ko'olau shield tholeiites (24–29, avg. 27 vs. 17–25; Salters et al., 2006). Based on these geochemical characteristics, we conclude that phlogopite was probably not an important residual phase in the source of the Koko Rift magmas. This is consistent with the relatively high degrees of melting implied by the weakly alkalic compositions of the Koko lavas, which should have exhausted residual minor phases such as phlogopite (Clague and Frey, 1982). In any case, phlogopite would likely have been only a minor residual phase in the source of the Koko Rift magmas and would not have a strong effect on trace element partitioning during melting. As such, we conclude that the Th-Ba-La compositions of the Koko basalts probably reflect primary geochemical characteristics of their mantle sources rather than effects of residual phases during melting. This interpretation is consistent with the conclusions of Yang et al. (2003).

The Ba enrichments in the Koko rocks, as indicated by their high Ba/Rb and Ba/Th ratios (Fig. 8) and seen in the primitive mantle normalized diagram of Clague et al. (2006), have implications for source compositions. Globally averaged MORB have Ba/Th ratios of (Gale et al., 2013), much lower than those measured for Koko Rift lavas (Fig. 8). The high Ba/Rb and Ba/Th ratios, and the Sr, Nd and Pb isotopic ratios for Koko Rift lavas (Fekiakova et al., 2007), preclude a MORB-like source for the Koko lavas. As high Ba/Th ratios are a general signature of Hawaiian plume basalts (Hofmann and Jochum, 1996; Norman and Garcia, 1999), the range of Ba/Th in the Koko Rift lavas may reflect variable enrichment of a depleted mantle reservoir, possibly either within or entrained by the plume, or at the base of the lithosphere, by incipient melts from the Hawaiian plume (Yang et al., 2003; Bizimis et al., 2005; Sen et al., 2011).

The Os isotopic compositions of Honolulu Volcanics provide additional insights into the source for Hawaiian rejuvenated lavas. The $^{187}Os/^{188}Os$ of these lavas range 0.1351–0.1598 with the Kaupo and Kalama flows having among the most radiogenic compositions (0.1503 and 0.1538; Lassiter et al., 2000). The combination of depleted (Sr-Nd-Pb) and enriched (Os) isotopic compositions clearly reflects diverse components in the source of these magmas. Lassiter et al. (2000)) interpreted these results as a product of mixing of melts from a mixed pyroxenite and peridotite source, both likely derived from the ~100 Ma Pacific lithospheric mantle. Sen et al. (2011) proposed that the

Table 7
New ICPMS trace element data for Koko Rift and Mānana Island samples.

Sample	K1–35	K1–38	Kaupo 1	Koko flow 3	Kalama 1	Lānaʻi Lookout	Mānana
Li	9.5	9.8	6.3	7.0	9.1	7.5	15.4
Be	1.6	1.7	1.1	1.3	1.4	1.6	3.0
Sc	25.4	26.1	24.7	23.7	23.0	22.6	25.1
Ti			12,169	13,074	13,838		
V	276	285	249	250	254	274	245
Cr			440	451	436		
Co	51	55	63	71	60	59	68
Ni	140	163	287	257	242	89	302
Cu	99	95	86	81	80	96	75
Zn	128	131	113	119	117	123	149
Ga	21.4	22.2	18.9	19.3	19.4	22.2	17.3
Rb	24.8	26.1	20.3	25.4	16.2	26.4	29.0
Sr	884	910	610	742	751	872	1432
Y	24.2	25.1	19.8	21.5	21.5	24.9	28.6
Zr	140	145	107	132	135	140	142
Nb	37.0	38.4	25.5	35.8	36.4	36.5	64.5
Cd			0.052	0.073	0.062		
Sn	2.0	1.7	1.3	1.5	1.6	1.6	1.4
Sb	0.078	0.059	0.030	0.039	0.053	0.046	0.324
Cs	0.35	0.37	0.19	0.28	0.13	0.35	0.52
Ba	525	556	361	480	500	553	1006
La	30.5	32.1	19.4	26.0	26.1	30.1	77.9
Ce	62.5	65.5	41.2	53.8	53.4	62.2	153
Pr	7.59	7.95	5.11	6.54	6.49	7.57	18.1
Nd	33.0	34.5	23.0	28.5	28.6	33.0	75.1
Sm	7.47	7.83	5.52	6.57	6.66	7.47	15.0
Eu	2.57	2.67	1.88	2.23	2.22	2.57	4.74
Gd	7.07	7.31	5.45	6.30	6.36	7.06	12.11
Tb			0.80	0.90	0.91		
Dy	5.39	5.62	4.23	4.71	4.70	5.55	7.28
Ho	0.96	1.00	0.79	0.85	0.86	0.99	1.15
Er	2.22	2.25	1.88	2.04	1.96	2.27	2.41
Yb	1.69	1.76	1.50	1.45	1.51	1.78	1.76
Lu	0.23	0.25	0.21	0.21	0.20	0.25	0.25
Hf	3.12	3.33	2.59	3.09	3.12	3.27	2.89
Ta	1.96	2.06	1.41	2.14	2.00	2.14	2.62
Pb	2.81	2.65	1.41	1.97	1.99	2.39	6.53
Th	3.38	3.52	1.99	2.84	2.78	3.30	9.36
U	0.90	0.94	0.43	0.74	0.93	0.86	2.43

All data in ppm.

radiogenic Os isotopic signature of Honolulu Volcanics was a consequence of the scavenging of intergranular sulfides during percolation of melt through the lithosphere. In contrast, the Pb isotopic compositions were thought to preclude a lithospheric mantle source (Fekiakova et al., 2007). Additional isotopic studies of the Honolulu Volcanics are necessary to clarify the nature of their mantle sources and their relationships to the Hawaiian plume.

9. Summary

The Koko Rift is the most recent (~67 ka), compositionally diverse and spectacular example of rejuvenation stage volcanism in Hawaii. It is 15 km long with 12 major and several minor subaerial and submarine eruptive centers. The lack of soils or erosional surfaces separating the deposits from these vents suggest the Koko eruptions were part of one magmatic sequence. The petrology of the lavas supports this interpretation. Two distinct compositional groups (high and low MgO) were erupted along the Koko Rift. The high MgO group (10–12.7 wt%) is similar to other Honolulu rejuvenation eruptions but is less alkaline and has much lower concentrations of incompatible elements such as Th. Previous studies have inferred the high MgO composition and the presence of mantle xenoliths in many Honolulu basalts as indicative of rapid ascent from mantle depths without crustal storage. The Koko Rift basalts had a different history involving crustal storage where the magma underwent variable degrees of crystal fractionation. Fractionation was following by magma mixing as indicated by reverse compositional zoning in olivine and clinopyroxene. Mixing involved at three magmas that are best preserved at the southern end of the Koko Rift.

The fractionated lavas with low MgO (5–7 wt%) are exceptional among Honolulu Volcanics and indicative of crustal storage prior to eruption. These lower MgO magmas erupted at the end of the eruptive sequence from several vents along the southern subaerial section of the Koko Rift. These lavas also show evidence of magma mixing with a higher MgO melt that probably triggered their eruption. Three compositionally distinct magmas and two mixing events are required to explain the diverse major and trace element trends among the Koko Rift lavas. Thus, the Koko Rift eruptive sequence was apparently unique among Hawaiian rejuvenated eruptions for its history of magma mixing and extensive crystal fractionation history.

The Mānana Island eruption preceded the Koko Rift eruptive sequence and produced a mineralogically distinctive, hauyne-bearing basalt.

Supplementary data to this article can be found online at https://doi.org/10.1016/j.jvolgeores.2022.107504.

Credit authorship contribution statement

Michael Garcia: Formal analysis, Investigation, Data curation, Writing - final draft, Funding acquisition, Supervision. Kierstin Swanson: Conceptualization, Data curation, Methodology, Writing- Original draft preparation. Charline Lormand: Formal analysis, Investigation, Reviewing and Editing. Marc Norman: Formal analysis, Data curation, Writing- Reviewing and Editing.

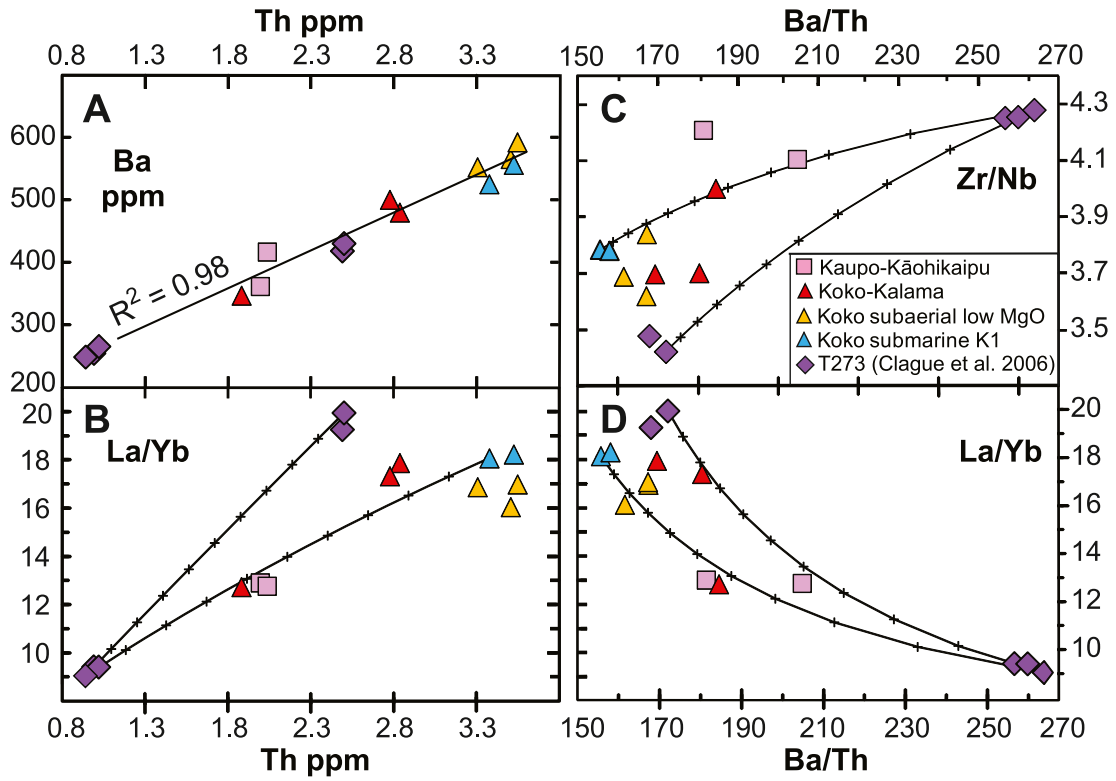

Fig. 8. Plots of ICPMS whole-rock, trace element data for Koko Rift basalts. A. The Th vs. Ba plot of data from four Koko Rift studies shows a good linear correlation ($R^2 = 0.98$) suggesting the interlaboratory differences are minor. Mixing curves have been modeled for panels B, C and D using the submarine basalt compositions. The pluses indicate 10% increments of mixing. B. The La/Yb vs. Th plot shows a large range in La/Yb with the southernmost submarine basalts (3 purple triangles, T273) forming one endmember and the other submarine basalts from the two other submarine cones forming other potential endmembers. The lower MgO lavas (gold triangles) have somewhat higher Th abundances that reflect crystal fractionation. C. Th/Ba vs. Zr/Nb plot showing two magma mixing trends. The subaerial samples fall within this mixing trends. D. The Ba/Th vs. La/Yb plot supports the magma mixing interpretation involving the submarine T273 submarine (purple triangles) and the K1 (light blue triangles) as potential mixing endmembers. (For interpretation of the references to colour in this figure legend, the reader is referred to the web version of this article.)

Declaration of Competing Interest

The authors declare that they have no known competing financial interests or personal relationships that could have appeared to influence the work reported in this paper.

Acknowledgements

We thank Mike Vollinger and Mike Rhodes for their diligent efforts in making the XRF analyses, Joe Boro for help with the BSE images in Fig. 6 and some of the microprobe analyzes, Tracy Ibara for obtaining water well data from the USGS that she used to make the Kalama flow map and do the volume calculations. Comments from two anonymous journal reviewers helped to improve the manuscript. The research was partially supported by NSF grant OCE-1834758 to MG. This is SOEST contribution no. 11471.

References

Bianco, T.A., Ito, G., Becker, J.M., Garcia, M.O., 2005. Secondary Hawaiian volcanism formed by flexural arch decompression. Geochem. Geophys. Geosyst. 6, Q08009 https://doi.org/10.1029/2005GC000945.

Bizimis, M., Sen, G., Salters, V.J., Keshav, S., 2005. Hf-Nd-Sr isotope systematics of garnet pyroxenites from Salt Lake Crater, Oahu, Hawaii: evidence for a depleted component in Hawaiian volcanism. Geochim. Cosmochim. Acta 69, 2629–2646.

Clague, D.A., 1987. Hawaiian xenolith populations, magma supply rates, and development of magma chambers | SpringerLink. Bull. Volcanol. 49, 557–587.

Clague, D.A., Frey, F.A., 1982. Petrology and trace element geochemistry of the Honolulu Volcanics, Oahu: implications for the Oceanic Mantle below Hawaii. J. Petrol. 23, 447–504.

Clague, D.A., Frey, F.A., Garcia, M.O., Huang, S., McWilliams, M., Beeson, M.H., 2016. Compositional heterogeneity of the sugarloaf melilite nephelinite flow, Honolulu Volcanics, Hawaii. Geochim. Cosmochim. Acta 185, 251–277. https://doi.org/10.1016/j.gca.2016.01.034.

Clague, D.A., Paduan, J.B., McIntosh, W.C., Cousens, B.L., Davis, A.S., Reynolds, J.R., 2006. A submarine perspective of the Honolulu Volcanics, Oahu. J. Volcanol. Geotherm. Res. 151, 279–307.

Conticelli, S., Boari, E., Avanzinelli, R., De Benedetti, A.A., Giordano, G., Mattei, M., Melluso, L., Morra, V., 2010. Geochemistry, isotopes and mineral chemistry of the Colli Albani volcanic rocks: constraints on magma genesis and evolution. "The Colli Albani Volcano", Special Publications of IAVCEI Geol. Soc. Lond. 3, 107–139.

Dana, J.D., 1890. Characteristics of Volcanoes with Contributions of Facts and Principles from the Hawaiian Islands. Dodd, Mead and Co., New York.

Dartnell, P., Gardner, J.V., 1999. Sea-floor images and data from multibeam surveys in San Francisco Bay, Southern California, Hawai'i, the Gulf of Mexico, and Lake Tahoe, California–Nevada. In: Digital Data Series DDS-55. U.S. Geol. Surv.

Fekiakova, Z., Abouchami, W., Galer, S.J.G., Garcia, M.O., Hofmann, A.W., 2007. Origin and temporal evolution of Ko'olau Volcano, Hawaii: Inferences from isotope data on the Koolau Scientific Drilling Project (KSDP), the Honolulu Volcanics and ODP Site 843. Earth Planet. Sci. Lett. 261, 65–83.

Fisher, R.V., 1977. Erosion by volcanic base-surge density currents: U-shaped channels. Bull. Geol. Soc. Am. 88, 1287–1297.

Gale, A., Dalton, C.A., Langmuir, C.H., Su, Y.J., Schilling, J.G., 2013. The mean composition of ocean ridge basalts. Geochem. Geophys. Geosyst. 14, 489–518.

Garcia, M.O., Pietruszka, A.P., Rhodes, J.M., Norman, M., 2021. Kīlauea's Pu'u 'Ō'ō Eruption (1983-2018): a synthesis of magmatic processes during a prolonged basaltic event. Chem. Geol. 581, 120391 https://doi.org/10.1016/j.chemgeo.2021.120391.

Guest, I., Ito, G., Garcia, M.O., Hellebrand, E., 2020. Extensive magmatic heating of the lithosphere beneath the Hawaiian Islands inferred from Salt Lake Crater mantle xenoliths. Geochem. Geophys. Geosyst. 21, e2020GC009359 https://doi.org/10.1029/2020GC009359.

Hoernle, K.A.J., Schmincke, H.U., 1993. The role of partial melting in the 15-Ma geochemical evolution of Gran Canaria: a blob model for the Canary hotspot. J. Petrol. 34, 599–626.

Hofmann, A.W., Jochum, K.P., 1996. Source characteristics derived from very incompatible trace elements in Mauna Loa and Mauna Kea basalts, Hawaii Scientific Drilling Project. J. Geophys. Res. 101, 11831–11839.
Hofmann, Albrecht W., White, William M., 1983. Ba, Rb and Cs in the Earth's Mantle. Zeitschrift Naturforschung A 38, 256–266. https://doi.org/10.1515/zna-1983-0225.
Jackson, E.D., Wright, T.L., 1970. Xenoliths in the Honolulu Volcanic Series, Hawaii. J. Petrol. 1, 405–430.
Jicha, B., Garcia, M.O., Lormand, C., 2022. The youngest rejuvenated volcanism in Hawai'i: A sea-level fall trigger and implications for future eruptions in Honolulu. Nat. Commun. (in review).
Jochum, K.P., Weis, U., Schwager, B., Stoll, B., Wilson, S.A., Haug, G.H., Andreae, M.O., Enzweiler, J., 2015. Reference values following ISO guidelines for frequently requested rock reference materials. Geostand. Geoanal. Res. 40, 333–350.
Kereszturi, G., Cappello, A., Ganci, G., Procter, J., Németh, K., Del Negro, C., Cronin, S.J., 2014. Numerical simulation of basaltic lava flows in the Auckland Volcanic Field, New Zealand—implication for volcanic hazard assessment. Bull. Volcanol. 76, 879. https://doi.org/10.1007/s00445-014-0879-6.
Krmíček, L., Halavinova, M., Romer, R.L., Galiova, M.V., Vaculovic, T., 2014. Phlogopite/matrix, clinopyroxene/matrix and clinopyroxene/phlogopite trace-element partitioning in a calc-alkaline lamprophyre: new constrains from the Krizanovice minette dyke (Bohemian Massif). J. Geosci. 59, 87–96.
Lassiter, J.C., Hauri, E.H., Reiners, P.W., Garcia, M.O., 2000. Generation of Hawaiian post-erosional lavas by melting of a mixed lherzolite/pyroxenite source: Implications for the chemical evolution of oceanic lithosphere. Earth Planet. Sci. Lett. 178, 269–284.
LaTourrette, T., Hervig, R.L., Holloway, J.R., 1995. Trace element partitioning between amphibole, phlogopite, and basanite melt. Earth Planet. Sci. Lett. 135, 13–30.
Macdonald, G.A., Abbott, A.T., Peterson, F.L., 1983. Volcanoes in the Sea. University of Hawaii Press, pp. 420–452.
Norman, M.D., Garcia, M.O., 1999. Primitive tholeiitic magma compositions and source characteristics of the Hawaiian plume: Constraints from picritic lavas. Earth Planet. Sci. Lett. 168, 19–26.
Ozawa, A., Tagami, T., Garcia, M.O., 2005. Unspiked K–Ar dating of the Honolulu rejuvenated and Koʻolau shield volcanism on Oʻahu, Hawaiʻi. Earth Planet. Sci. Lett. 232, 1–11.
Paul, D., White, W.M., Blichert-Toft, J., 2005. Geochemistry of Mauritius and the origin of rejuvenescent volcanism on oceanic island volcanoes. Geochem. Geophys. Geosyst. 6.
Peslier, A.H., Bizimis, M., Matney, M., 2015. Water disequilibrium in olivines from Hawaiian peridotites: recent metasomatism, H diffusion and magma ascent rates. Geochim. Cosmochim. Acta 154, 98–117. https://doi.org/10.1016/j.gca.2015.01.030.
Pukui, M.K., Elbert, S.H., Mookini, E.T., 1976. Place Names of Hawaii: Revised and Expanded Edition. University of Hawaii Press, Honolulu, p. 320.
Rhodes, J.M., Vollinger, M.J., 2004. Composition of basaltic lavas sampled by phase-2 of the Hawaii Scientific Drilling Project: geochemical stratigraphy and magma types. Geochem. Geophys. Geosyst. 5, Q03G13. https://doi.org/10.1029/2002GC000434.
Roeder, P.L., Emslie, R.F., 1970. Olivine-liquid equilibrium. Contrib. Mineral. Petrol. 29, 275–289. https://doi.org/10.1007/BF00371276.
Rottas, K.M., Houghton, B.F., 2012. Structure, stratigraphy, and eruption dynamics of a young tuff ring: Hanauma Bay, Oʻahu, Hawaiʻi. Bull. Volcanol. 74, 1683–1697.
Salters, V.J., Blichert-Toft, J., Fekiacova, Z., Sachi-Kocher, A., Bizimis, M., 2006. Isotope and trace element evidence for depleted lithosphere in the source of enriched Koʻolau basalts. Contrib. Mineral. Petrol. 151, 297–312.
Satow, C., Gudmundsson, A., Gertisser, R., Ramsey, C.B., Bazargan, M., Pyle, D.M., Wulf, S., Miles, A.J., Hardiman, M., 2021. Eruptive activity of the Santorini Volcano controlled by sea-level rise and fall. Nat. Geosci. 14, 586–592.
Schmidt, K.H., Bottazzi, P., Vannucci, R., Mengel, K., 1999. Trace element partitioning between phlogopite, clinopyroxene and leucite lamproite melt. Earth Planet. Sci. Lett. 168, 287–299.
Sen, G., Keshav, S., Bizimis, M., 2005. Hawaiian mantle xenoliths and magmas: Composition and thermal character of the lithosphere. Am. Mineral. 90, 871–887.
Sen, I.S., Bizimis, M., Sen, G., Huang, S., 2011. A radiogenic Os component in the oceanic lithosphere? Constraints from Hawaiian pyroxenite xenoliths. Geochim. Cosmochim. Acta 75, 4899–4916.
Stearns, H.T., Vaksvik, K.N., 1935. Geology and groundwater resources of the island of Oahu, Hawaii. Bull. Hawaii Div. Hydrography 1, 479 p.
Stille, P., Unruh, D.M., Tatsumoto, M., 1983. Pb, Sr, Nd and Hf isotopic evidence of multiple sources for Oahu, Hawaii basalts. Nature 304, 25–29.
Szabo, B.J., Ludwig, K.R., Muhs, D.R., Simmons, K.R., 1994. Thorium-230 ages of corals and duration of the last interglacial sea-level high stand on Oahu, Hawaii. Science 266, 93–96.
Weis, D., Frey, F.A., Giret, A., Cantagrel, J.M., 1998. Geochemical characteristics of youngest volcano (Mount Ross) in the Kerguelen Archipelago; inferences for magma flux, lithosphere assimilation and composition of the Kerguelen Plume. J. Petrol. 39, 973–994.
Wentworth, C.K., 1926. Pyroclastic geology of Oahu: B. P. Bishop. Mus. Bull. 30, 121 p.
Wentworth, C.K., 1951. Geology and Ground-Water Resources of the Honolulu-Pearl Harbor Area Oahu, Hawaii. Honolulu Board of Water Supply, 111 p.
Winchell, H., 1947. Honolulu Series, Oahu, Hawaii. Geol. Soc. Am. Bull. 58, 1–48.
Wright, E., White, W.M., 1987. The origin of Samoa; new evidence from Sr, Nd, and Pb isotopes. Earth Planet. Sci. Lett. 81, 151–162.
Yang, H.-J., Frey, F.A., Clague, D.A., 2003. Constraints on the source components of lavas forming the Hawaiian North Arch and Honolulu Volcanics. J. Petrol. 44, 603–627.